THE HYDROLYSIS OF HYDROXAMIC ACID COMPLEXANTS IN THE PRESENCE OF NON-OXIDISING METAL IONS 1: FERRIC IONS

F.P.L.Andrieux[a], C.Boxall*[a], R.J.Taylor[b]

[a]Centre for Materials Science, University of Central Lancashire, Preston PR1 2HE, UK

[b]Nexia Solutions Ltd, British Technology Centre, Sellafield, Seascale, Cumbria CA20 1PG, UK

*To whom all correspondence should be sent. Centre for Materials Science, University of Central Lancashire, Preston PR1 2HE, UK. Tel.: +44 1772 893530; fax: +44 01772 892996. E-mail: cboxall@uclan.ac.uk

Abstract

Hydroxamic acids (XHAs) are organic compounds with affinities for cations such as Fe^{3+}, Np^{4+} and Pu^{4+} and have been identified as useful reagents in nuclear fuel reprocessing. Acid catalysed hydrolysis of free XHAs is well known and may impact negatively on reprocessing applications. Hydrolysis of metal bound XHAs within metal ion-XHA complexes is less understood. With the aid of speciation diagrams, we have modelled UV-visible spectrophotometric kinetic studies of the acid-catalysed hydrolysis of acetohydroxamic acid (AHA) bound to the model ion Fe(III). These studies have yielded the following for the hydrolysis of AHA in the $Fe(AHA)^{2+}$ complex at 293 K:

(i) the order with respect to $[H^+]$ during the rate determining step, m = 0.97, the same as for the free ligand, indicating a similarity of mechanism; and

(ii) the rate parameter, $k_1=1.02 \times 10^{-4}$ $dm^3 \bullet mol^{-1} \bullet s^{-1}$, greater than that for the free ligand, $k_0 = 1.84 \times 10^{-5}$ $dm^3 \bullet mol^{-1} \bullet s^{-1}$ for pH > -0.5, a result consistent with a Hammett analysis of the system.

Keywords

Acetohydroxamic acid, ferric ions, complexation, speciation, hydrolysis, kinetics

1. Introduction

The separation of U from Np and Pu are major stages in the reprocessing of spent nuclear fuel by the Purex process [1,2]. Separation is commonly achieved by oxidation state-specific aqueous / non-aqueous solvent extraction processes, controlled by redox manipulation of key Pu or Np oxidation states or by the use of hydrophilic complexing agents e.g. sulphate ions. Simple hydroxamic acids (XHA) are salt free, hydrophilic organic compounds with the formula RCONHOH and so can act as di-oxygen ligands with affinities for 'hard' cations such as Fe^{3+}, Np^{4+} and Pu^{4+} [3-6] with which they form 5-membered chelate rings. They are also redox active, capable of reducing a range of metal ions - for instance they very rapidly reduce Np(VI) to Np(V) [7]. These two properties have led to them being identified as useful reagents for the control of Pu and Np in an Advanced Purex and UREX processes [2,6,8-9].

Acid hydrolysis of free hydroxamic acids to hydroxylamine (itself a reducing agent for a range of actinide species [10,11]) and the parent carboxylic acid is well known [12]. The kinetics of the hydrolysis of formohydroxamic acid (FHA, R=H) and acetohydroxamic acid (AHA, R=CH_3) in nitric acid have been determined [13] and are found, at $[HNO_3] < 3$ mol•dm^{-3} and when $[HNO_3] > [XHA]$, to obey eq. 1:

$$-\frac{d[XHA]}{dt} = Ae^{-\frac{E_A}{RT}}[XHA][H^+] \quad (1)$$

where, for FHA and AHA respectively, A, the pre-exponential factor, is 9.09×10^9 and 3.22×10^9 dm^3 •mol^{-1} •s^{-1} and E_A, the activation energy, is 77.3 and 79.9 kJ •mol^{-1}. Hydrolysis of metal ion bound-hydroxamates also occurs. Additionally, preliminary studies have shown that the Pu(IV)-FHA and AHA complexes are slowly reduced to free Pu(III) ions [9]. An understanding of these processes is vital if they are to be

controlled within the design of an XHA-based Advanced Purex process. To this end, we have experimentally studied and theoretically modelled the kinetics of the hydrolysis of metal-XHA systems in nitrate media where (i) the metal ion complexes with, but does not oxidise the ligand (Fe^{3+} / AHA; Np^{4+} / FHA, Np^{4+}/AHA); (ii) the metal ion both complexes and oxidises the ligand (Pu^{4+} / FHA and Pu^{4+} / AHA). This paper reports our findings with respect to an example of the first class of experiments i.e. the hydrolysis of an XHA in the presence of a complexing, but non-oxidising metal ion – specifically the hydrolysis of AHA (structure shown in **I**) in the presence of Fe^{3+} ions.

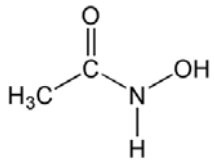

I – acetohydroxamic acid (AHA)

The experiments and kinetic modelling protocols developed will subsequently be used in similar studies of Np(IV)-XHA systems or adapted for use in the study of the Pu(IV)-XHA systems. The findings of the Np(IV)-XHA and Pu(IV)-XHA experiments will form the bases of the next two papers in this series.

2. Experimental Methods

2.1. Materials

All reagents, including HNO_3 (70%, AnalaR, BDH Chemicals Ltd., Poole, Dorset, UK), AHA (98%, Sigma-Aldrich Ltd, UK) and iron(III) nitrate nonahydrate (>99%, AnalaR, BDH Chemicals Ltd., Poole, Dorset, UK) were obtained from reputable suppliers at the

highest available purity and used as received. AHA was stored in a conventional refrigerator at 4°C in order to prevent its decomposition. Solutions of AHA were prepared immediately prior to experiment. Solutions were prepared using doubly distilled water, produced by a home-made still and further purified by a deionisation system (E pure model 04642, Barnstead / Thermodyne, Dubuque, Iowa, USA) to a resistivity of 1.8×10^5 Ω m.

2.2. Procedures

UV-visible absorbance spectra of complex and complex precursor solutions were measured by spectrophotometry (Diode Array model 8452A, Hewlett Packard, USA) fitted with a HP89090A Peltier temperature controller.

For kinetic experiments, a single wavelength spectrophotometer (Model SP6-350, Pye-Unicam, UK) was set to measure absorbance at $\lambda = 498$ nm, the absorption maximum of the mono-acetohydroxamato complex (vide infra). Solutions for the kinetic experiments were prepared from stock (Fe(III)) or freshly made solutions (AHA) and pipetted into an optical cuvette (pathlength 1 cm). The complexant (AHA) was added last. The volume of complexant required was always small and had no effect on the temperature of the receiving solution when added. After mixing, the absorbance was then measured manually at appropriate time intervals.

All experiments were conducted at 293 ± 1 K. All experiments involving Fe(III) were conducted at pH < 2.5. However, it is well known that Fe^{3+} readily hydrolyses in water in accordance with:

$$Fe^{3+} + H_2O \Leftrightarrow FeOH^{2+} + H^+$$

this equilibrium being the first step in a series of deprotonation / polymerisation reactions that ultimately result in the formation of ferric hydroxides and oxyhydroxides. Using the most recently published, critically assessed Gibbs energies of formation of the various species involved [14,15], the equilibrium constant for this first deprotonation can be calculated as being equal to 6.78×10^{-3}, corresponding to a $pK_a(Fe^{3+})$ of 2.17. Thus, as hydrolysis to form $Fe(OH)^{2+}$ will become significant above pH = 2.17, only those data recorded at pH = 2.1 and below will be subjected to rigorous experimental interpretation and modelling. Data recorded in the range $2.1 < pH < 2.5$, where shown, is presented for the purposes of context only.

3. Results and Discussion

3.1. Speciation and Kinetic Modelling of Metal-Hydroxamic Acid Systems

The ferric-AHA system exhibits three complexes at AHA:Fe ratios of 1:1, 2:1, 3:1. All three are intensely coloured being purple (λ_{max} = 498 nm), red-brown (λ_{max} = 460 nm) and orange-brown (λ_{max} = 440 nm) respectively. Interconversions between the free metal and the complexes can be described by the following [16,17], all at 298 K:

$$HL + Fe^{3+} \Leftrightarrow FeL^{2+} + H^{+} \qquad K_1 = 109 \qquad (2a)$$

$$HL + FeL^{2+} \Leftrightarrow FeL_2^{+} + H^{+} \qquad K_2 = 2.04 \qquad (2b)$$

$$HL + FeL_2^{+} \Leftrightarrow FeL_3 + H^{+} \qquad K_3 = 7.4 \times 10^{-3} \qquad (2c)$$

where HL = hydroxamic acid, L = hydroxamate anion.

The dynamics of the hydrolysis of the metal-AHA system in HNO_3 media are complicated by the speciation of the complex. Thus, in order to aid data treatment, speciation diagrams were calculated for the Fe(III)-AHA systems at 298 K at a range of [AHA], pH and pHL, Figs.1 & 2, where pH = $-\log_{10}[H^+]$ and pHL = $-\log_{10}$[AHA].

We assume the following mechanism in modelling the hydrolysis of XHA in the presence of non-oxidising ions such as Fe(III) and Np(IV) – and that the dominant form of the complex is the mono-hydroxamato species ML.

$$HL + M \xleftrightarrow{K_1} C + H^{+} \qquad (3)$$

$$HL + H^{+} \xrightarrow{k_0} RCOOH + NH_3OH^{+} \qquad (4)$$

$$C + mH^{+} \xrightarrow{k_1} M + RCOOH + NH_3OH^{+} \qquad (5)$$

where M = $[Fe^{3+}]$ or $[Np^{4+}]$ and M_t = $[Fe^{3+}]$ or $[Np^{4+}]$ at time t; (6a)

HL_t = [XHA] at time t; (6b)

C_t = [metal ion-XHA complex] at time t; (6c)

$k'_1 = k_1[H^+]^m$ assumed by analogy with (6d)

$k'_0 = k_0[H^+]$ in accordance with eq. 1. (6e)

The equilibrium described by K_1 is given by:

$$K_1 = \frac{C}{M\ HL\ \lfloor H^+ \rfloor} \quad (7)$$

The forward and back reactions associated with eqs. 2 are assumed to be fast on the timescale of XHA hydrolysis and so at equilibrium throughout the experiment. Further, given that the pK_a of both hydroxamic acids investigated in this study and subsequent papers in this series are greater than 8.5 [18] (pK_a (FHA) = 8.78; pK_a (AHA) = 9.02), under the conditions employed in the experiments described below (pH < 2.5), the dominant form of the free ligand will be the acid rather than the deprotonated conjugate base. Thus, direct hydrolysis of the hydroxamate ion may be neglected. Mass balance on the metal cation, the ligand and nitrate anion at times t and t=0 demand that:

$HL_{T,0} = HL_0 + C_0$ $\qquad$ $HL_{T,t} = HL_t + C_t$ (8a,b)

$M_T = M_0 + C_0$ $\qquad$ $M_T = M_t + C_t$ (8c,d)

$[NO_3^-]_T = [NO_3^-] + MNO_3$ (8e)

where $[NO_3^-]_T$, MNO_3, M_T, $L_{T,t}$ and $L_{T,0}$ represent the total concentration of nitrate, concentration of metal ion-complexed nitrate (vide infra), total concentration of metal cation, total concentration of ligand (free or in complex) at time t and total concentration of ligand (free or in complex) at time t=0 respectively. Eq. 8b gives:

$$\frac{dHL_{T,t}}{dt} = \frac{dHL_t}{dt} + \frac{dC_t}{dt} \quad (9)$$

Similarly, eqs. 1, 6d and 6e give:

$$\frac{dHL_{T,t}}{dt} = k_0[H^+]HL_t + k_1[H^+]^m C_t = k'_0\, HL_t + k'_1\, C_t \quad (10)$$

Eqs. 7 and 8d give:

$$C_t = \frac{K'_1\, HL_t M_T}{[H^+] + K'_1\, HL_t} \quad (11)$$

where $K'_1 = K_1$ and $K'_1 = \frac{K_1}{1 + ([NO_3^-]_T / K_D)}$ (12a,b)

for non-nitrate-complexing metal ions such as Fe^{3+} and nitrate-complexing actinide(IV) species, respectively. The latter is included to support the application of this model in the actinide metal ion-XHA systems to be described in subsequent papers in this series [19]. The parameter K_D describes the dissociation of the weak complex formed between e.g. Np(IV) and NO_3^- via:

$$Np(NO_3)^{3+} \Leftrightarrow NO_3^- + Np^{4+} \quad (12c)$$

Differentiation of eq. 11 and substitution into eq. 9 gives:

$$\frac{dHL_{T,t}}{dt} = \frac{dHL_t}{dt}\left(1 + \frac{K'_1[H^+]M_T}{([H^+] + K'_1\, HL_t)^2}\right) \quad (13)$$

Substitution of eq. 11 into 10 and substituting the result into eq. 13 then gives:

$$\frac{dHL_t}{dt} = -HL_t \frac{\left(k'_0 + \frac{k'_1 K'_1 M_T}{[H^+] + K'_1\, HL_t}\right)}{\left(1 + \frac{K'_1[H^+]M_T}{([H^+] + K'_1\, HL_t)^2}\right)} \quad (14)$$

Full solution of eq. 14 gives:

$$t = \frac{1}{k'_1}\ln\left(\frac{\frac{K'_1 HL_t}{[H^+]}+1}{\frac{K'_1 HL_0}{[H^+]}+1}\right) - \left(\frac{\frac{K'_1 M_T}{[H^+]}+1}{\frac{k'_1 K'_1 M_T}{[H^+]}+k'_0}\right)\ln\left(\frac{HL_t}{HL_0}\right) - \left(\frac{\frac{k'^2_1 K'_1 M_T}{[H^+]}+k'^2_0}{\frac{k'_0 k'^2_1 K'_1 M_T}{[H^+]}+k'^2_0 k'_1}\right)\ln\left(\frac{\frac{K'_1 HL_t}{[H^+]}+1+\frac{k'_1 K'_1 M_T}{k'_0[H^+]}}{\frac{K'_1 HL_0}{[H^+]}+1+\frac{k'_1 K'_1 M_T}{k'_0[H^+]}}\right) \quad (15)$$

where HL_0 may be obtained by solving the quadratic produced by substitution of eq. 11 into eq. 8a at t=0. Eq. 15 is insoluble with respect to HL_t. However, it can be used to calculate theoretical HL_t *vs* t and, through eq. 11, C_t *vs* t plots. Curve fitting these to experimental data allows for the extraction of values of key parameters such as $k'_1 = k_1[H^+]^m$ as a function of $[H^+]$. A plot of $\log_{10}(k_1[H^+]^m)$ *vs* $\log[H^+]$ then allows calculation of values of m and k_1.

3.2 Experimental Study of the Iron-Acetohydroxamic Acid System

Figs.1 & 2 allow for the recording of separate UV-visible spectra under conditions when $Fe(AHA)^{2+}$, $Fe(AHA)_2^+$ and $Fe(AHA)_3$ are the dominant complex species. Examples of such spectra are shown in Fig.3. These allow the identification of λ_{max} values for $Fe(AHA)^{2+}$ and $Fe(AHA)_2^+$ of 498 nm and 460 nm respectively. Use of Fig.3 in conjunction with Figs.2b, 1a and 1b allows for the calculation of the following extinction coefficients:

For $Fe(AHA)^{2+}$, $\varepsilon = 1070\ dm^3 \bullet mol^{-1} \bullet cm^{-1}$ at $\lambda_{max} = 498$ nm; $\varepsilon = 913\ dm^3 \bullet mol^{-1} \bullet cm^{-1}$ at $\lambda = 460$ nm.

For $Fe(AHA)_2^+$, $\varepsilon = 932\ dm^3 \bullet mol^{-1} \bullet cm^{-1}$ at $\lambda_{max} = 460$ nm; $\varepsilon = 774\ dm^3 \bullet mol^{-1} \bullet cm^{-1}$ at $\lambda = 498$ nm.

Figs.1 & 2 also show that, at $M_T = 0.0025\ mol \bullet dm^{-3}$ and pHL > 2.4, the mono-acetohydroxamato-Fe(III) complex forms >90% of all complexed Fe at pH < 1.5, so

defining the [AHA] and pH range over which kinetic experiments may be conducted wherein, for ease of analysis, complexed Fe exists near-exclusively as the $Fe(AHA)^{2+}$ complex.

With these experimental and analytical restrictions in mind, and in order to test the range of utility of the various assumptions made, acetohydroxamato-Fe(III) complex hydrolysis experiments were conducted at 293 K at a total iron concentration of 0.0025 $mol \bullet dm^{-3}$, a total AHA concentration of 0.004 $mol \bullet dm^{-3}$ (AHA:Fe ratio = 1.6:1) and at $pH \leq 2.5$, although it should be borne in mind that experiments conducted in the range $2.1 < pH \leq 2.5$ may be complicated by the hydrolysis of Fe^{3+} to form $Fe(OH)^{2+}$. The results of these experiments are shown in Fig.4. Taken from Fig.4, Fig.5 shows the initial absorbance due to complexed Fe^{3+} at $\lambda = 498$ nm, as a function of pH, data at $pH > 2.1$ having been discarded due to quantitative analysis being complicated by the potential formation of $Fe(OH)^{2+}$. Superimposed over this data set are three theoretical absorbance traces, all calculated at $\lambda = 498$ nm using the speciation data of Fig.2b:

(i) the absorbance due to the 1:1 complex calculated using $\varepsilon = 1070\ dm^3 \bullet mol^{-1} \bullet cm^{-1}$

(ii) the absorbance due to the 2:1 complex calculated using $\varepsilon = 774\ dm^3 \bullet mol^{-1} \bullet cm^{-1}$

(iii)the sum of both absorbances.

There is reasonable correspondence between the calculated total and experimental absorbance values. Comparison of the calculated total absorbance trace and that calculated trace due to $Fe(AHA)^{2+}$ indicates that, under the experimental conditions employed, the 1:1 complex is responsible for >90% of the measured absorbance at $pH < 1.7$. This supports the analysis above that at $M_T = 0.0025\ mol \bullet dm^{-3}$ and pHL > 2.4, the 1:1 complex forms >90% of all complexed iron at $pH < 1.5$. The absorbance measured

for all data recorded at pH < 1.7 is therefore predominantly due to $Fe(AHA)^{2+}$, so allowing use of the experimental model described by eqs. 7-15 and data analysis by curve fitting with eqs. 11 and 15. This curve fitting is facilitated by the observation of k_1 and K'_1 having different effects on the shape of the calculated C_t vs t curve. These effects are illustrated in Fig.6 and may be qualitatively understood as follows.

The rate parameter k_1 affects the overall duration of the decrease in concentration of complex with time, although this effect is found to vanish for very small values of k_1. This is readily understood in that once the process associated with k_1 (eq. 5) is much slower than the parallel process associated with k_0 (eq. 4) (i.e. $k_1[H^+]^m << k_0[H^+]$), the latter process determines the overall rate. In contrast, no matter the overall duration of the decay in complex concentration, the equilibrium constant K'_1 only affects the degree of sigmoid character in the C_t vs t profile with a pseudo-induction period appearing at large K'_1 during which C_t is invariant with time. The larger K'_1 at any one set of otherwise constant experimental conditions, the longer the induction period before the concentration starts to decay. Again, this may be readily understood in that the larger K'_1, the longer a significant / measurable concentration of complex will maintain during the overall decay time. Curve fitting the data of Fig.4 is further facilitated by only one parameter being unknown in this instance: k'_1 (= $k_1[H^+]^m$, eq. 6d). Using Fig.4, the curve fitting procedure can be conducted on data recorded as a function of $[H^+]$, so allowing m and k_1 to be determined from a plot of $\log_{10}k'_1$ vs $\log_{10}[H^+]$ (eq. 6d).

Fig.7 shows the data of Fig.4, normalised with respect to the absorbance at t=0, and associated theoretical fits generated using eqs. 11 and 15, also normalised with respect to the calculated $[Fe(AHA)^{2+}]$ at t=0. Parameters used in the generation of each fitting

plot are listed in table 1. Data at pH 2.5 have again been excluded from quantitative analysis due to potential complications arising from $Fe(OH)^{2+}$ formation. Of particular interest are:

- at all pH bar –0.7, $k_1[H^+]^m > k_0[H^+]$ indicating that complexed acetohydoxamate is more susceptible to acid-catalysed hydrolysis than free AHA.
- k_1 has a negative value at pH –0.7 – this will be explored below.

From table 1 and in accordance with eq. 6d, Fig.8 shows a plot of $\log_{10} (k_1[H^+]^m)$ vs $\log_{10}[H^+]$, excluding data at pH 2.5 (*vide supra*) and 2.01 (outside the range where the monoacetohydroxamato complex can be assumed to be the dominant form of complexed ferric ions) and pH –0.7 (due to the above-mentioned negative value of k_1). The slope and intercept of the plot in Fig.8 give values of m and k_1 of 0.97 and 1.02 x 10^{-4} $dm^3 \bullet mol^{-1} \bullet s^{-1}$ respectively.

According to Monzyk and Crumbliss, the forward and back reactions associated with eq. 2a have rate coefficient values of 2 x 10^3 and 7.6 x 10^{-2} dm^3 mol^{-1} s^{-1} respectively [17]. As the rate coefficients for the hydrolysis of free AHA and AHA within the 1:1 complex are 1.84 x 10^{-5} (see table 1) and 1.02 x 10^{-4} dm^3 mol^{-1} s^{-1} respectively, our earlier assumption of the reaction associated with eq. 2a being at equilibrium throughout the experiments reported here can be seen to be justified. This validates the use of eqs. 11 and 15 in the analysis of the data of Figs.4 and 7.

The negative value of k'_1 obtained at pH = -0.7 is due to the lower pH limit of applicability of eq. 1 being approximately pH –0.5. This limit is thought to arise from a possible change in the mechanism of acid-catalysed hydrolysis of *free* AHA at or around pH –0.5. The mechanism at pH > -0.5 has long been thought to involve [12]:

(i) rapid pre-equilibrium protonation of the carbonyl oxygen; followed by

(ii) nucleophilic attack by water at the carbonyl carbon, resulting in the formation of a tetrahedral intermediate; followed by

(iii) re-creation of carbonyl at the new tetrahedral C with loss of leaving group NH_2OH (see Fig.9).

Taylor *et al* report that in nitric acid (< 3 mol•dm^{-3}), XHAs hydrolyse in accordance with this mechanism to give hydroxylamine and the parent carboxylic acid, the rate obeying eq. 1 [13]. Modena *et al* have also investigated the hydrolysis of propanhydroxamic acid in sulphuric and nitric acid and found that both acids exert an identical catalytic effect with the rates passing through a maximum as a function of $[H^+]$ [20]. Buglass and Juffkins have reported a similar rate maximum in a series of studies on 2,2-dimethylacetohydroxamic acid [21]. This experimental rate maximum is therefore a departure from the applicability of eq. 1 at high $[H^+]$, with k'_0 values calculated using eq. 1 at pH < -0.5 being greater than those obtained by experiment – so accounting for the negative value of $k'_1 = k_1[H^+]^m$ obtained in table 1. Several explanations have been forwarded to explain this change in mechanism and which of these, if any, are true is still uncertain [12]:

(a) rate saturation at high $[H^+]$ due to complete conversion of the (weakly) basic substrate into its conjugate acid;

(b) the acid-base pre-equilibrium steps and transition state formation steps being governed by different acidity functions;

(c) a change in the initial protonation site from the carbonyl O to the hydroxylamino N (see Fig.9).

It is our view that it is the first of these explanations that is most applicable for the system studied here. Whilst experiments are underway in our laboratories to verify this view, an early indication of its validity is provided by the data of Fig.10 which again presents the experimental data recorded at pH –0.7 from Fig.7. However, in this instance, rather than taking the literature value of K'_1, a value of k'_0 calculated in accordance with eq. 1 and then obtaining the best fit by variation of k'_1, k'_1 has first been calculated using eq. 6d and the values of m and k_1 of 0.97 and 1.02 x 10^{-4} dm^3 $\bullet mol^{-1}$ $\bullet s^{-1}$ obtained above. The theoretical fit has then been obtained by varying k'_0 within eqs. 11 and 15. The fit shown in Fig.10 was obtained using a value of k'_0 of 5.51 x 10^{-5} s^{-1}, which is less than the value of k'_0 = 9.2 x 10^{-5} s^{-1} calculated by use of eqs. 1 and 6e at pH –0.7. Eq. 1 predicts a value of the second order rate constant k_0 of 1.84 x 10^{-5} dm^3 $\bullet mol^{-1}$ $\bullet s^{-1}$ (see table 1). Dividing the fitted value of k'_0 of 5.51 x 10^{-5} s^{-1} by k_0 = 1.84 x 10^{-5} dm^3 $\bullet mol^{-1}$ $\bullet s^{-1}$ gives a value of $[H^+]$ = 3 mol$\bullet dm^{-3}$, this despite the experiment having been conducted at pH –0.7, corresponding to $[H^+]$ = 5.01 mol$\bullet dm^{-3}$.

This effective value of $[H^+]$ = 3 mol$\bullet dm^{-3}$, corresponding to pH –0.48, is coincident with the upper limit of applicability of eq. 1 reported by Taylor et al [13] and the acidity at which Buglass and Juffkins report that the rate of hydrolysis of 2,2-dimethylacetohydroxamic acid saturates [21]. In light of this result, we suggest that of the three above suggested explanations of the hydrolytic behaviour of free AHA at low pH, explanation (a) is the most likely to obtain i.e. that deviation from eq. 1 at high acidity is caused by a saturation in the protonation of carbonyl group of AHA to form its conjugate acid $AHAH^+$. According to the generally accepted mechanism (i)-(iii) above, $AHAH^+$ is then the species that undergoes nucleophilic attack by water to form the observed reaction products. Consequently, the measured rate of hydrolysis of free

AHA would be expected to be proportional to the instantaneous concentration of $AHAH^+$.

From table 1 it is apparent that complexation of AHA with Fe^{3+} to form a 1:1 complex accelerates the hydrolysis of AHA at pH > -0.5 at 293 K. This can be understood by first noting that m = 1 for the hydrolysis of both the free and bound AHA, suggesting that the same general mechanism obtains in each system at pH > -0.48 i.e. rapid pre-equilibrium protonation of the carbonyl oxygen of the bound AHA is followed by nucleophilic attack by water on the carbonyl carbon (mechanism (i)-(iii) above). With this in mind, acceleration by complexation at pH > -0.5 is consistent with the observation that, through a Hammett equation analysis, electron withdrawing substituents (X in XHA, the metal in the hydroxamato-metal complex) accelerate the hydrolysis of AHA by increasing the susceptibility of the carbon of the hydroxamate carbonyl group to nucleophilic attack by H_2O.

It is of interest to note that, at $1.48 \geq pH \geq 0.49$, k_1 is approximately 5.6x greater than k_0. Table 2 compares the hydrolytic half life of free AHA, $(t_{½})_0$, with that of AHA in the presence of Fe^{3+} as determined from the experimental data of Fig.7. This comparison indicates that hydrolysis in the presence of Fe^{3+} is at most 3x faster than that of free AHA, reflecting the incomplete complexation of AHA with ferric ions. The greatest difference between the rate ratio expected on the basis of k_1/k_0 with that determined experimentally is seen at low pH, reflecting the lower levels of mono-acetohydroxamato complex formed at high acidities (Fig.2b).

Finally, let us return to our conclusion that the deviation at pH < -0.48 of the measured value of k'_0 from that calculated using eq. 1 is due to complete conversion of AHA into

its conjugate acid $AHAH^+$ (explanation (a) above). If such a secenario were to obtain then a speciation diagram of the type shown in Fig.11 would apply. Concentrations of $AHAH^+$ and AHA over the pH range shown are then given by

$$[AHAH^+] = \frac{[H^+]}{K_A + [H^+]}[AHA]_T \quad (16a)$$

$$[AHA] = \frac{K_A}{K_A + [H^+]}[AHA]_T \quad (16b)$$

where $[AHA]_T = [AHA] + [AHAH^+]$ and K_A is the equilibrium constant for:

$$AHAH^+ \Leftrightarrow AHA + H^+ \quad (17)$$

Eq. 16a has two asymptotic forms. At high pH, $[H^+] < K_A$ and eq. 16a reduces to:

$$[AHAH^+] = \frac{[H^+]}{K_A}[AHA]_T \quad (18a)$$

which, if the rate of free AHA hydrolysis is taken to be proportional to $[AHAH^+]$ (vide supra) is consistent with the experimental dependence of that rate on total AHA concentration and $[H^+]$ given in eq. 1. At low pH, $[H^+] > K_A$ and eq. 16a reduces to:

$$[AHAH^+] = [AHA]_T \quad (18b)$$

and the rate becomes invariant with pH. Eq. 16 and eq. 18a therefore suggest that k'_0 for hydrolysis of the free ligand is most appropriately written as

$$k'_0 = \frac{k_0^H}{[H^+] + K_A}[H^+] \approx k_0[H^+] \quad (19a)$$

where k_0^H is the pseudo-first order rate coefficient for the nucleophilic attack of water on free $AHAH^+$. An analogous equation can be written for the complexed ligand:

$$k'_1 = \frac{k_1^H}{[H^+] + K_{A,C}}[H^+] \approx k_1[H^+] \quad (19b)$$

where $K_{A,C}$ is the equilibrium constant for the process analogous to eq. 17 that occurs with complexed AHA.

Returning to the free ligand, schematic plots of eq. 16a, 18a and 18b are shown in Fig.12 from which it can be seen that, at the point of intersection of the plots derived from asymptotic eqs. 18a and 18b, $[H^+] = K_A$. From eq. 19a, it can be seen that this value of $[H^+]$ can also be determined by dividing the value of k_0 calculated from eq. 1 into the (saturation) value of k'_0 obtained by the curve fitting of Fig.10. Consequently, K_A for the equilibrium given by eq. 17 can be seen to have a value of 3 mol•dm^{-3}. Fig.11 shows the speciation diagram obtained from eqs. 16 using K_A = 3 mol•dm^{-3}and a total concentration of acetohydroxamic acid = 0.0025 mol•dm^{-3}.

In using the data of Fig.10 in this computation of K_A, we are necessarily assuming that the protonation of the carbonyl oxygen in the *complexed* ligand has yet to achieve saturation at pH –0.7 i.e. $k'_1 = k_1[H^+]$ where $k_1 = 1.02 \times 10^{-4}$ dm^3 •mol^{-1} •s^{-1} obtained above. This is not unreasonable as AHA complexation with Fe^{3+} to form a complex of the type shown in Fig.9 will necessarily make the lone pairs on the carbonyl oxygen less available for protonation. Thus $K_{A,C}$ for the complexed ligand will be greater than K_A for the free, with the degree of ligand protonation and so level of hydrolytically active $AHAH^+$ formation being suppressed upon complexation. Returning to table 1, comparison of k'_1 with k'_0 in the context of eqs. 19 and the deduction that $K_{A,C} > K_A$, then indicates that $k_1^H > k_0^H$ i.e. that the rate of nucleophilic attack of water on the carbonyl carbon is greater for complexed than free $AHAH^+$. This deduction is consistent with the Hammett-based analysis above i.e. that electron withdrawing groups on the carbonyl will increase the susceptibility of the carbonyl carbon to nucleophilic attack.

4. Conclusions

Acid catalysed hydrolysis of free XHAs is well known and may impact negatively upon their potential applications in spent nuclear fuel reprocessing. Hydrolysis of the metal bound ligand within metal ion-XHA complexes is less well understood. In order to elucidate the effect of complexation on the hydrolysis reaction, we have with the aid of speciation diagrams, modelled and explained UV-visible spectrophotometric kinetic studies of the acid-catalysed hydrolysis of acetohydroxamic acid (AHA) whilst bound to the model ion Fe(III). Kinetic models have been developed and used to obtain the following for the hydrolysis of AHA in the $Fe(AHA)^{2+}$ complex at 293 K:

(i) the second order rate parameter, $k_1=1.02 \times 10^{-4}$ $dm^3 \bullet mol^{-1} \bullet s^{-1}$; and

(ii) the order with respect to $[H^+]$ during the rate determining step, m = 0.97.

The latter indicates that the mechanism for the hydrolysis of complexed AHA is analogous to that of the free ligand i.e. rapid pre-equilibrium protonation of the carbonyl oxygen (pK_a = -0.48) followed by nucleophilic attack by water on the carbonyl carbon.

The value of the former, k_1, is greater than the analogous parameter for hydrolysis of the free ligand, $k_0 = 1.84 \times 10^{-5}$ $dm^3 \bullet mol^{-1} \bullet s^{-1}$ at all pH > -0.5. This is consistent with a Hammett-based analysis wherein electron withdrawing groups (the metal during complexation) accelerate AHA hydrolysis by increasing the susceptibility of the carbonyl group to nucleophilic attack.

Acknowledgements

The authors wish to thank British Nuclear Fuels Ltd and the Nuclear Decommissioning Authority (NDA) for financial support and for a post-doctoral research fellowship for FA.

References

[1] Dennis, I.S., Jeapes, A.P., Reprocessing Irradiated Fuel. In: Wilson, P.D., Ed., The Nuclear Fuel Cycle, Oxford Science Publications, Chapter 7, p.116, 1996.

[2] Birkett, J.E., Carrott, M.J., Fox, O.D., Jones, C.J., Maher, C.J., Roube, C.V., Taylor, R.J., Woodhead, D.A.: Recent Developments in the Purex Process for Nuclear Fuel Reprocessing: Complexant Based Stripping for Uranium - Plutonium Separation. Chimia 59, 898-904 (2005).

[3] Desaraju, P., Winston, A.: Synthesis and Iron Complexation Studies of Bis-Hydroxamic Acids. J.Co-ord.Chem. 14, 241-248 (1986).

[4] Barocas, A., Baroncelli, F., Biondi, G.B., Grossi, G.: The Complexing Power of Hydroxamic Acids and its Effects on Behaviour of Organic Extractants in the Reprocessing of Irradiated Fuels II. J.Inorg.Nucl.Chem. 28, 2961-2967 (1966).

[5] Baroncelli, F., Grossi, G.: The Complexing Power of Hydroxamic Acids and its Effects on Behaviour of Organic Extractants in the Reprocessing of Irradiated Fuels I. J.Inorg.Nucl.Chem. 27, 1085-1092 (1965).

[6] Taylor, R.J., May, I., Wallwork, A.L., Dennis, I.S., Hill, N.J., Galkin, B.Y., Zilberman, B.Y., Fedorov, Y.S.: The Applications of Formo- and Aceto- Hydroxamic Acids in Nuclear Fuel Reprocessing. J.Alloys Comp. 271-273, 534-537 (1998).

[7] Colston, B.J.; Choppin, G.R.; Taylor, R.J. A preliminary study of the reduction of Np(VI) by formohydroxamic acid using stopped-flow near-infrared spectrophotometry. Radiochimica Acta 88, 329-334 (2000).

[8] Fox, O.D., Jones, C.J., Birkett, J.E., Carrott, M.J., Maher, C.J., Roube, C.V. Taylor, R.J.: Advanced PUREX flowsheets for future Np and Pu fuel cycle demands. In: Separations for the Nuclear Fuel Cycle in the 21st Century; Lumetta, G.J, Nash, K.L., Clark, S.B., Friese, J.I., Eds. ACS Symposium Series 933, ACS, Washington DC. USA, 89-102, 2006.

[9] Todd, T.A., Wigelund, R.A., Advanced Separation Technologies for Processing Spent Nuclear Fuel and the Potential Benefits to a Geologic Repository. In: Separations for the Nuclear Fuel Cycle in the 21st Century; Lumetta, G.J, Nash, K.L., Clark, S.B., Friese, J.I., Eds. ACS Symposium Series 933, ACS, Washington DC. USA, 41-56, 2006.

[10] Koltunov, V.S., Zhuravleva, G.I., Shapovalov, M.P.: Kinetics of Actinide Reduction by hydroxylamine 5 & 6. Soviet Radiochem. 23, 449-453 & 454-459 (1981).

[11] Barney, G.S.: A Kinetic Study of the Reaction of Plutonium(IV) with Hydroxylamine. J.Inorg.Nucl.Chem. 38, 1677-1681 (1976).

[12] Ghosh, K.K.: Kinetic and Mechanistic Aspects of Acid Catalysed Hydrolysis of Hydroxamic Acids. Indian J.Chem. 36B, 1089-1102 (1997).

[13] Carrott, M.J., Fox, O.D., Jones, C.J., Mason, C., Taylor, R.J., Sinkov, S.I., Choppin, G.R.: Solvent Extraction Behaviour of Plutonium Ions in the Presence of Simple Hydroxamic Acids, Solvent Extraction and Ion Exchange, to be submitted (2007)

[14] Cornell, R.M., Schwertmann, U.: The Iron Oxides, VCH Publishers, New York, Chapter 8, p. 175, 1996.

[15] Heusler, K.E., Lorenz, W.J., Standard Potentials in Aqueous Solution, Bard, A.J., Parsons, R., Jordan, J., Eds., Marcel Dekker Inc., New York, Chapter 14, p.391, 1985.

[16] Kazmi, S.A., McArdle, J.V.: Kinetics of Formation of Bis- and Tris(acetohydroxamato) Fe(III). J.Inorg.Nucl.Chem. 43, 3031-3034 (1981).

[17] Monzyk, B., Crumbliss, A.L.: Mechanism of Ligand Substitution on High-Spin Iron(III) by Hydroxamic Acid Chelators. Thermodynamic and Kinetic Studies on the Formation and Dissociation of a Series of Monohydroxamatoiron (III) Complexes. J.Am.Chem.Soc., 101:21, 6203 (1979).

[18] Martell, A.E., Smith, R.M.: Critical Stability Constants, National Institute of Standards, Standard Reference Database 46, Version 6.0 (2001).

[19] Andrieux, F.P.L., Boxall, C., Mason, C., Taylor, R.J.: The Hydrolysis of Hydroxamic Acid Complexants in the Presence of Non-Oxidising Metal Ions 2: Neptunium (IV) Ions. J.Solution Chem., submitted (2007).

[20] Di Furia, F., Modena, G., Scrimin, P., Gasparini, G.M., Grossi, G.: The Role of Hydroxamic Acids in the Retention of Fission Products in TBP Diluents. A Quantitative Study in a Model System. Sep.Sci.Tech. 17, 1451-1468 (1982).

[21] Buglass, A.J., Dorr, M., Juffkins, M.: On the Rate Maxima Observed in the Acid Hydrolysis of Some Alkylhydroxamic Acids. Tet.Letts. 28, 3283-3284 (1987).

Figure Captions

Figure 1. Speciation diagrams for Fe^{3+} - AHA system at 298 K showing concentrations of Fe^{3+}, FeL^{2+}, FeL_2^{+} and FeL_3 (data series 1-4 respectively in all figures) as functions of total AHA concentration (expressed as pHL) calculated at total [Fe(III)] = 0.0025 mol•dm^{-3} and [HNO_3] = (a) 0.01 mol•dm^{-3}; (b) 0.1 mol•dm^{-3}; (c) 1 mol•dm^{-3} and (d) 6 mol•dm^{-3}.

Figure 2. Speciation diagrams for Fe^{3+} - AHA system at 298 K showing concentrations of Fe^{3+}, FeL^{2+}, FeL_2^{+} and FeL_3 (data series 1-4 respectively in all figures) as functions of pH calculated at total [Fe(III)] = 0.0025 mol dm^{-3} and total [AHA] = (a) 0.0025 mol•dm^{-3}; (b) 0.004 mol•dm^{-3}; (c) 0.025 mol•dm^{-3}, corresponding to AHA:Fe ratios of 1:1, 1.6:1, 10:1 respectively.

Figure 3. UV-visible absorption spectra of Fe-AHA system recorded in HNO_3 solution. Fe^{3+} and AHA spectra recorded as indicated in legend. (a) $Fe(AHA)^{2+}$ spectrum recorded from 4.2 x 10^{-4} mol•dm^{-3} solution of complex produced, as calculated from Fig. 1b, from a solution of 2.5 x 10^{-3} mol•dm^{-3} Fe^{3+} and 4 x 10^{-3} mol•dm^{-3} AHA at pH 1.16, λ_{max} = 498 nm. (b) $Fe(AHA)_2^{+}$ spectrum recorded from 2.23 x 10^{-3} mol•dm^{-3} solution of complex produced, as calculated from Fig.1a, from a solution of 2.5 x 10^{-3} mol•dm^{-3} Fe^{3+} and 0.16 mol•dm^{-3} AHA at pH 2, λ_{max} = 460 nm. For both (a) and (b) the spectra of AHA recorded in isolation were found to be featureless over the wavelength range shown.

Figure 4. Absorbance of 0.0025 mol•dm^{-3} Fe^{3+}, 0.004 mol•dm^{-3} AHA solution (AHA:Fe(III) ratio = 1.6:1) as f(t) measured at 293 K, λ_{max} = 498 nm. Experiments

conducted in HNO_3 solution, data series 1 – 7 recorded at pH 2.5, 2.01, 1.48, 1.16, 0.79, 0.49 and –0.7 respectively.

Figure 5. Series 1: Plot of initial (t=0) absorbance vs pH for data of Fig. 4. Series 2: Plot of total theoretical absorbance due to $Fe(AHA)^{2+}$ and $Fe(AHA)_2^{+}$ complexes vs pH, calculated using Fig. 2b and $\varepsilon = 1070$ $dm^3 \bullet mol^{-1} \bullet s^{-1}$ for $Fe(AHA)^{2+}$ and $\varepsilon = 774$ $dm^3 \bullet mol^{-1} \bullet s^{-1}$ for $Fe(AHA)_2^{+}$. Series 3: Plot of theoretical absorbance due to $Fe(AHA)^{2+}$ only vs pH. Series 4: Plot of theoretical absorbance due to $Fe(AHA)_2^{+}$ only vs pH.

Figure 6. Normalised C_t vs t calculated using eqs. 15 and 11. All data series calculated for AHA using $M_T = 0.005$ $mol \bullet dm^{-3}$, $HL_T = 0.1$ $mol \bullet dm^{-3}$, pH = 0, $k_0 = 1.836 \times 10^{-5}$ $dm^3 \bullet mol^{-1} \bullet s^{-1}$ and m=1. (a) $k_1 = 2 \times 10^{-3}$ $dm^6 \bullet mol^{-2} \bullet s^{-1}$, data series 1-4 corresponding to $K'_1 = 25, 100, 250, 1000$ respectively. (b) $K'_1 = 250$, data series 1-6 corresponding to $k_1 = 1 \times 10^{-3}$, 5×10^{-4}, 2.5×10^{-4}, 1×10^{-4}, 1×10^{-5}, 1×10^{-6} $dm^6 \bullet mol^{-2} \bullet s^{-1}$ respectively.

Figure 7. Theoretical (calculated using eqs. 11 & 15) and experimental (taken from Fig.4) plots of normalised $[Fe(AHA)^{2+}]$ vs t for a mixture of 0.0025 $mol \bullet dm^{-3}$ Fe^{3+} and 0.004 $mol \bullet dm^{-3}$ AHA (total AHA:Fe(III) ratio = 1.6:1) at 293 K. Experiments conducted in nitric acid solution, Experimental data series 1 produced at pH 2.5. Experimental data series 2-7 and theoretical data series 8-13 produced at pH 2.01, 1.48, 1.16, 0.79, 0.49 and –0.7 respectively. Theoretical data series produced using exact values of k'_1 given in table 1.

Figure 8. Plot of $\log (k_1[H^+]^m)$ vs $\log ([H^+])$ for data of table 1.

Figure 9. Schematic summary of effects of nucleophilic attack of H_2O on Fe(III)-AHA complex protonated at the carbonyl oxygen or hydroylamino nitrogen.

Figure 10. Theoretical (calculated using eqs. 11 & 15) and experimental (taken from Fig.7) plots of normalised $[Fe(AHA)^{2+}]$ vs t for a mixture of 0.0025 mol•dm^{-3} Fe^{3+} and 0.004 mol•dm^{-3} AHA (total AHA:Fe(III) ratio = 1.6:1) at 293 K. Experiment conducted in nitric acid solution, pH –0.7. Theoretical data series produced using $k_1 = 1.02 \times 10^{-4}$ dm^3•mol^{-1}•s^{-1} (calculated from Fig.8) and $k'_0 = 5.51 \times 10^{-5}$ s^{-1} (as a fitting parameter).

Figure 11. Schematic speciation diagram for AHA system at 298 K showing concentrations of $AHAH^+$ and AHA (data series 1 and 2 respectively) as a function of pH. Total AHA concentration (= [AHA] + $[AHAH^+]$) = 0.0025 mol•dm^{-3}. K_A = 3 mol•dm^{-3}.

Figure 12. Schematic plots of $[AHAH^+]$ vs $[H^+]$ calculated using eq. 16a, 18a ($[H^+] < K_A$) and 18b ($[H^+] > K_A$).

Tables

pH	k_0 / $dm^3 \bullet mol^{-1} \bullet s^{-1}$ from eq. 1	$k'_0 = k_0[H^+]$ / s^{-1} from eq. 6e	K_1 $=K'_1$	M_T / $mol \bullet dm^{-3}$	HL_T / $mol \bullet dm^{-3}$	$k'_1 = k_1[H^+]^m$ / s^{-1} from Fig.4 & eqs. 11 & 15
2.01	1.84×10^{-5}	1.79×10^{-7}	109	0.0025	0.004	1.90×10^{-6}
1.48	1.84×10^{-5}	6.08×10^{-7}	109	0.0025	0.004	3.97×10^{-6}
1.16	1.84×10^{-5}	1.27×10^{-6}	109	0.0025	0.004	6.43×10^{-6}
0.79	1.84×10^{-5}	2.98×10^{-6}	109	0.0025	0.004	2.11×10^{-5}
0.49	1.84×10^{-5}	5.94×10^{-6}	109	0.0025	0.004	3.17×10^{-5}
-0.7	1.84×10^{-5}	9.2×10^{-5}	109	0.0025	0.004	-6.26×10^{-4}

TABLE 1. Values of $k'_0 = k_0[H^+]$ (calculated using eqs. 1 and 6e) and $k'_1 = k_1[H^+]^m$ (from data of Fig.4 and eqs. 11 & 15) as a function of pH at 293 K.

pH	$k'_0 = k_0[H^+]$ / s^{-1} from table 1 & eqs. 1 & 6e	$(t_{½})_0 = \ln 2 / k'_0$ / s from col. 2	$(t_{½})_{expt}$ / s from Fig.7	$(t_{½})_0/(t_{½})_1$
1.48	6.08×10^{-7}	11.52×10^5	3.77×10^5	3.05
1.16	1.27×10^{-6}	5.46×10^5	2.46×10^5	2.22
0.79	2.98×10^{-6}	2.33×10^5	0.89×10^5	2.62
0.49	5.94×10^{-6}	1.16×10^5	0.63×10^5	1.84

TABLE 2. Comparison of half life values, $t_{½}$, as a function of pH at 293 K for (i) hydrolysis of free AHA, $(t_{½})_0$, obtained using k'_0 value calculated from eq. 1 and (ii) hydrolysis of AHA in the presence of Fe^{3+} ions, $(t_{½})_{expt}$, experimentally determined from the data of Fig.7.

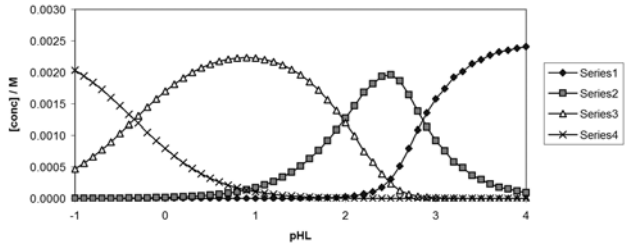

FIGURE 1a

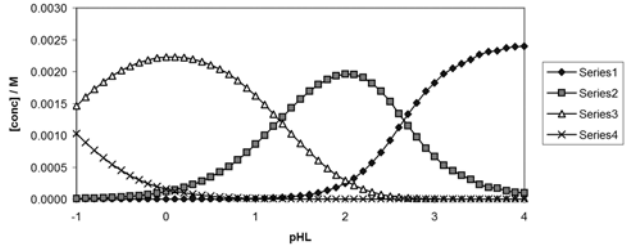

FIGURE 1b

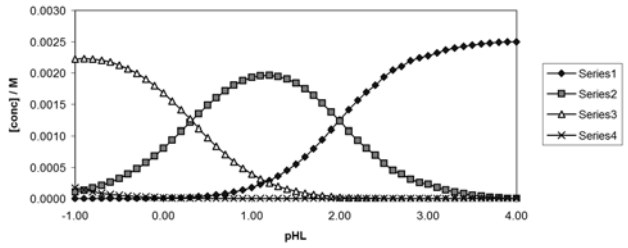

FIGURE 1c

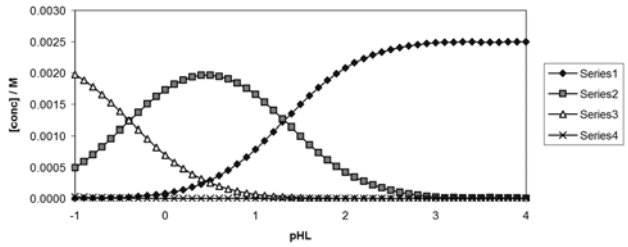

FIGURE 1d

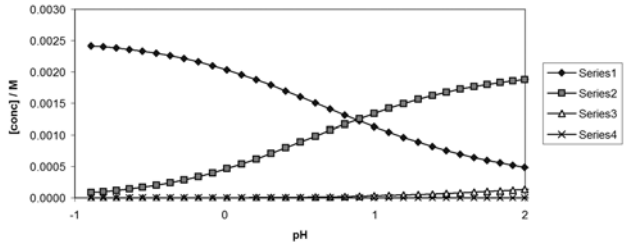

FIGURE 2a

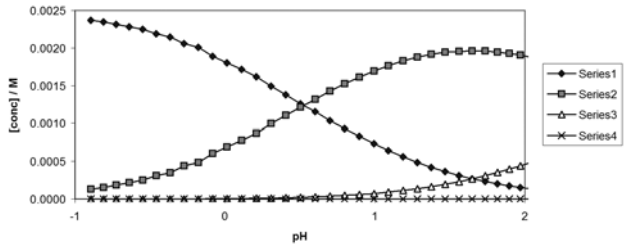

FIGURE 2b

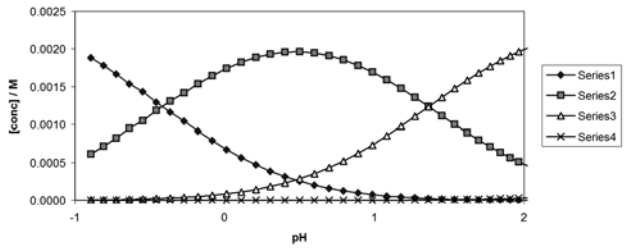

FIGURE 2c

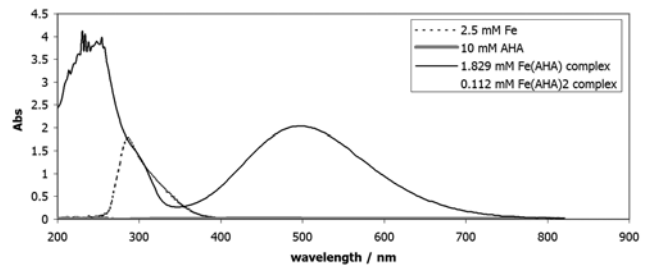

FIGURE 3a

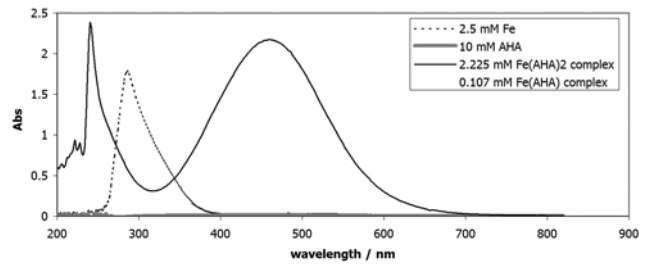

FIGURE 3b

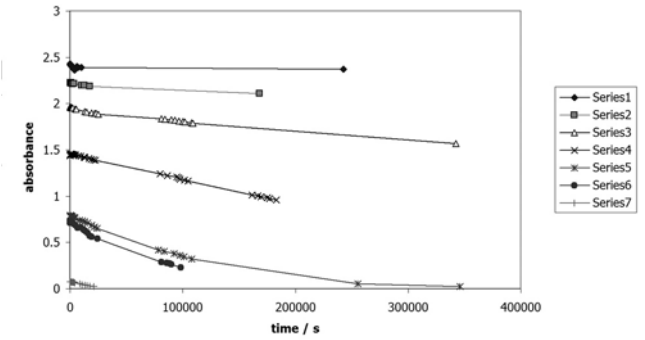

FIGURE 4

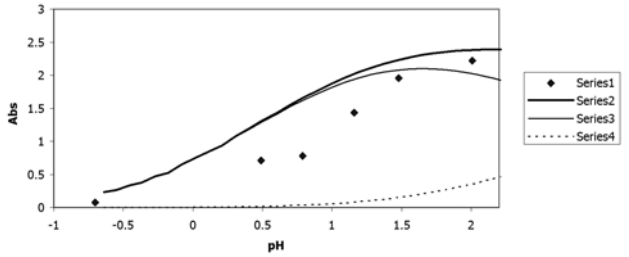

FIGURE 5

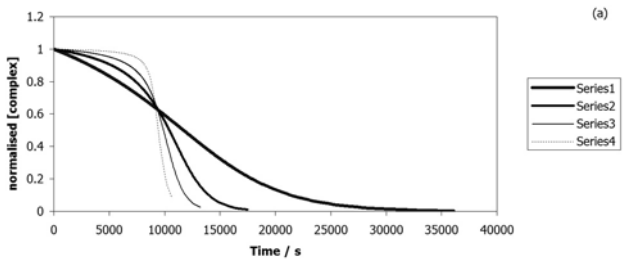

FIGURE 6a

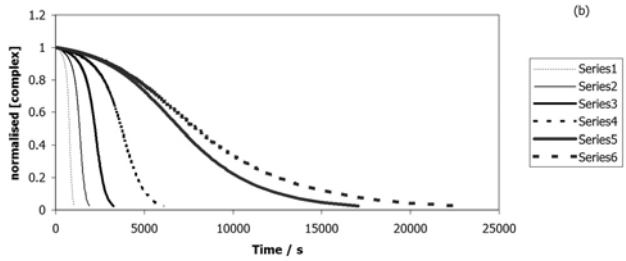

FIGURE 6b

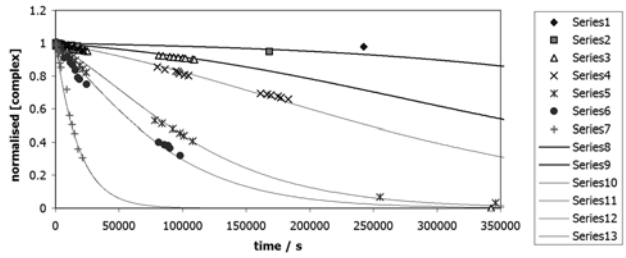

FIGURE 7

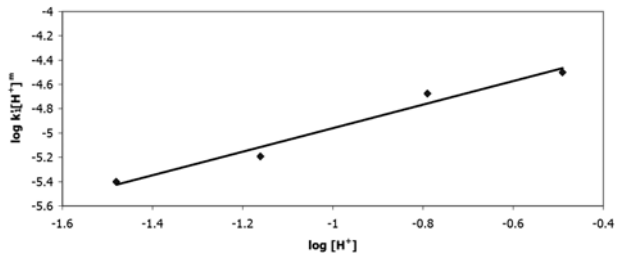

FIGURE 8

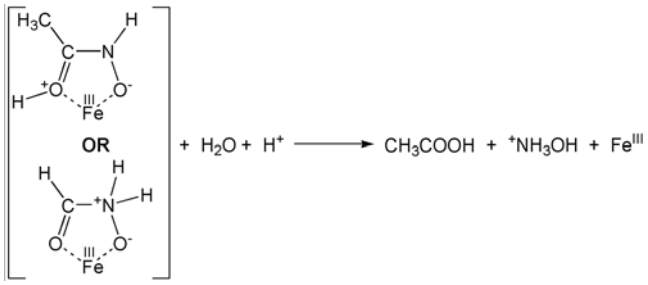

FIGURE 9

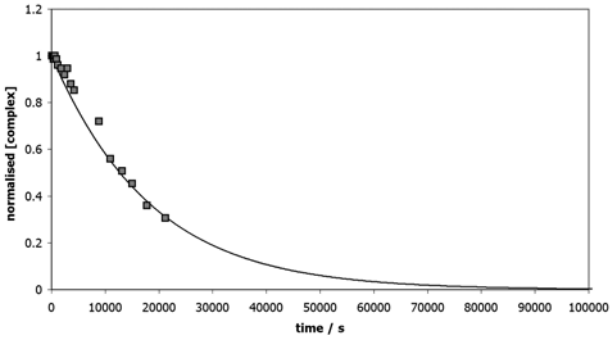

FIGURE 10

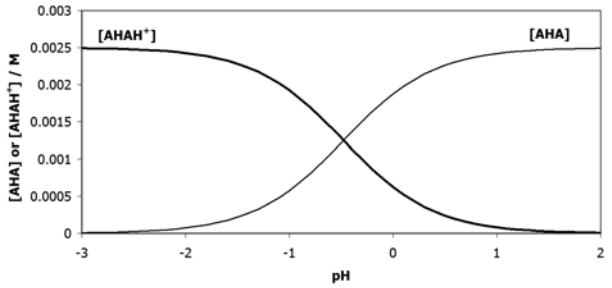

FIGURE 11

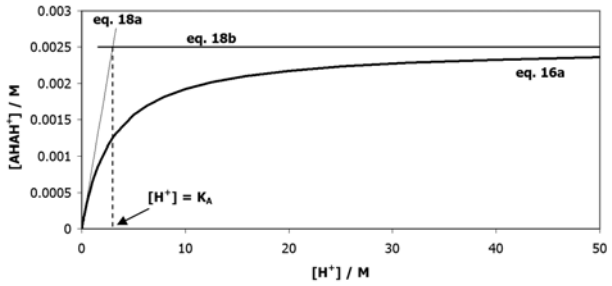

FIGURE 12